A novel and versatile solar Borehole Thermal Energy Storage assisted by a Heat Pump. Part 1: System description

Charles Maragna, Charlotte Rey, Marc Perreaux

Renewable Energy 208 (2023) 709–725

Contents lists available at ScienceDirect

Renewable Energy

journal homepage: www.elsevier.com/locate/renene

A novel and versatile solar Borehole Thermal Energy Storage assisted by a Heat Pump. Part 1: System description

Charles Maragna [a,*], Charlotte Rey [b], Marc Perreaux [b]

[a] BRGM, France
[b] STORENGY, France

ARTICLE INFO

Keywords:
Renewable heating
Borehole thermal energy storage
Heat pump
Solar thermal collectors
Domestic hot water

ABSTRACT

The paper reports a system combining Solar Thermal Collectors (STC), Borehole Thermal Energy Storage (BTES), a Heap Pump (HP) and a backup boiler for space heating and Domestic Hot Water (DHW) production. The integration of the components and the overall control strategy are described. The system is flexible, being able to select the best thermal source and to use it directly or through a HP, while only the excess solar heat is stored into the BTES. The contribution of every subsystem to the energy mix is discussed. For a "reference configuration" combining the three subsystems ("Design D") and characterized by heating and DHW needs of 510.5 MWh.y^{-1} and 226.7 MWh.y^{-1} respectively, a BTES volume of 15000 m^3, a distance between boreholes of 3 m, a STC area of 2500 m^2, and a solar tank volume of 100 m^3, the system uses 274 units of gas and electricity to provide 1000 units of heating and DHW. This reference configuration outperforms any alternative design: Design A (STC only), Design B (STC and HP) and design C (STC and BTES) would respectively require 612, 480 and 591 units of gas and electricity to do so. A one-at-a-time analysis reveals that the STC area, azimuth and inclination, the solar tank volume, the BTES volume, the borehole density and the HP power are key parameters to the overall system performance.

1. Introduction

Heating and cooling in residential, service and industry sectors accounts for c.a. 50% of the EU's primary energy supply [1,2]. The EU-28 residential heating CO_2 emissions was estimated to be c.a. 500 × 10^6 ton CO_2/y from 2010 to 2015 [3], about 15% of the overall EU-27 emissions in 2018 [4]. Solutions must be urgently deployed to decarbonize energy supply in buildings.

Underground Thermal Energy Storage (UTES) mobilize a huge volume of soil to store low-carbon heat (e.g. waste or solar in summer) and retrieves it to shave the peaks in demand often associated with fossil fuel consumption. In a High Temperature Borehole Thermal Energy Storage (HT-BTES), a heat-carrier fluid circulates in plastic U-tube pipes installed in a large number of closely spaced (e.g. 3 m) 20–200 m deep Borehole Heat Exchangers (BHE). The ground is warmed up to a much higher temperature than its initial temperature (e.g. from 12 °C to 50–80 °C). Conversely, in a Low Temperature BTES (LT-BTES) a reversible Heat Pump (HP) makes the ground temperature oscillate by 10–15 °C around its initial value to produce heating and cooling [5]. LT-BTES is out of the scope of this paper. A bunch of HT-BTES demo sites are operational, including Solar Drake Landing, Okotoks, Canada [6], Neckarsulm, Germany [7], Emmaboda, Sweden [8], Brædstrup, Denmark [9]. A comprehensive overview of these demo sites can be found in Refs. [9,10].

Numerical models have been widely used to assess the thermal behaviour of BTES and their integration. Many studies used TRNSYS, a graphics-based software for the simulation of transient systems where modules (so-called "Types") are connected [11]. Sibbit et al. developed a TRNSYS model to design Solar Drake Landing through the maximization of the economic performance by tuning the area of Solar thermal Collectors (STC), the buffer tank size, and the number and depth of BHE [12]. The Solar Drake Landing design was translated into six climates to assess the subsequent solar fraction and BTES efficiency [13], and an alternative design reducing costs was proposed in Ref. [14]. Based on geometrical considerations, Lanini et al. derived an optimal

Abbreviations: **BHE** Borehole Heat Exchangers, **BTES** Borehole Thermal Energy Storage; **CHPP** Combined Heat and Power Plant, **DHN** District Heating Networks; **DHW** Domestic Hot Water, **FE** Finite Elements; **HT-BTES** High Temperature Borehole Thermal Energy Storage, **LT-BTES** Low Temperature Borehole Thermal Energy Storage; **HP** Heat Pumps, **STC** Solar Thermal Collectors; **TRT** Thermal Response Test, **UTES** Underground Thermal Energy Storage.

* Corresponding author. BRGM, 3 av. Claude-Guillemin, BP 36009 45060, Orléans, Cedex 2, France.
E-mail address: c.maragna@brgm.fr (C. Maragna).

https://doi.org/10.1016/j.renene.2023.03.105
Received 30 January 2023; Received in revised form 20 March 2023; Accepted 23 March 2023
Available online 27 March 2023

Nomenclature

Latin Letters

e	thickness [m]
E	energy [J]
$\dot{m}$	flow rate [kg.s^{-1}]
r	radius
R	thermal resistance [K.m.W^{-1}]
P	power [W]
T	temperature [°C]
t	time [s]

Greek letters

λ	thermal conductivity [W.K^{-1}.m^{-1}]
ρC_p	volume-specific heat capacity [J.K^{-1}.m^{-3}]
θ	STC slope (0 = horizontal, 90 = vertical facing the azimuth)
φ	azimuth

Subscripts

0	initial
b	borehole

Superscripts

E^*	normalized energy (i.e. divided by the total thermal demand)

Quantity Abbreviation

Thermal energy demand E_{demand}
Heating $E_{heating}$
Domestic Hot Water E_{DHW}
Direct solar energy for heating $E_{dir,sol,heating}$
Direct solar energy for DHW $E_{dir,sol,DHW}$
Frigorific energy used by solar HP for heating $E_{frig,sol,heating}$
Frigorific energy used by solar HP for DHW $E_{frig,sol,DHW}$
Electricity used by solar HP for heating $E_{el,sol,heating}$
Electricity used by solar HP for DHW $E_{el,sol,DHW}$
Direct BTES energy for heating $E_{dir,\ BTES,heating}$
Direct BTES energy for DHW $E_{dir,\ BTES,DHW}$
Frigorific energy used by BTES HP for heating $E_{frig,\ BTES,heating}$
Frigorific energy used by BTES HP for DHW $E_{frig,\ BTES,DHW}$
Electricity used by solar HP for heating $E_{el,BTES,\ heating}$
Electricity used by solar HP for DHW $E_{el,BTES,DHW}$
External backup for heating (to meet the heating setup temperature) $E_{backup,\ heating}$
External backup for DHW (to meet the DHW setup temperature = 40 °C) $E_{backup,DHW}$
Internal boost of DHW tank to 65 °C (once a day to prevent microbiological development) $E_{boost,DHW}$
Thermal loss on the heating tank $E_{heating,\ tank,loss}$
Thermal loss on the DHW tank $E_{DHW,\ tank,loss}$
Thermal loss on the solar tank $E_{solar,\ tank,loss}$
Collected solar energy transferred into the solar tank $E_{coll,\ solar}$
Solar energy transferred into the BTES $E_{load,\ BTES}$
Variation of internal energy of the solar tank $E_{int,\ solar,tank}$
Amount of electricity and backup needed to produce heating and DHW (including pumps) E_{ext}
Amount of electricity and backup needed to produce heating and DHW (excluding pumps) $E_{ext,\ w/o\ pumps}$

volume/depth ratio for BTES [15]. Guo et al. built a whole TRNSYS model of a 500 000 m^3 BTES storing industrial waste heat in Chifeng, Inner Mongolia, China [16]. This BTES was able to store 9.2 GWh in 90 days. Once the ground thermal properties have been calibrated from early recording, the model proved to be in very good agreement with measurements, i.e. the loading reported in Ref. [10]. Tordrup et al. used TRNSYS to back-calculate the key parameters of the elements composing Brædstrup BTES installation [17]. Using analytic solutions, Durga et al. optimized the boreholes number, depth and spacing of a BTES to store waste summer steam from a Combined Heat and Power Plant (CHPP) and retrieve it with a high temperature HP [18]. Rosato et al. analyzed the performance of 8 variants of a solar hybrid district heating network integrated with a seasonal BTES and connected to the electrical grid [19]. Panno et al. analyzed the energy flows and operating costs of a HP coupled to a solar BTES for a school located in southern Italy with a TRNSYS model [20]. They stated that connecting the solar field directly to the evaporators of the HP systems greatly decreases both the dimensions of the BTES and the solar field and consequently the initial investment cost. Elhashmi et al. studied a similar system for multi-family residences in Midwestern United States and concluded that an optimally-sized system would reduce energy consumption and carbon emission by 46% [21]. Note that the Domestic Hot Water (DHW) need was slightly higher than the heating need, which may be explained by the compactness of the considered residential buildings. Welsch et al. compared 7 BTES combinations (with or without STC and CHPP) for District Heating Networks (DHN) for 4 different economic scenarios [22]. They generated "Pareto fronts", i.e. the designs with the best cost vs. CO_2 emissions for 4 macro-economic scenarios and concluded that a combination of STC and BTES with a small CHPP is the best solution and is economical even without subsidies. Formhals et al. generated similar Pareto fronts for the integration of STC and BTES into an existing DHN, considering five rates of retrofitting [23]. Ciampi et al. modelled a system combining STC, a water tank, a BTES and a gas boiler for 6 single houses located in Naples [24]. Three specific parameters involving gross solar collector area, water tank volume and BTES volume were defined and, assuming 3 values per parameters, the best configurations from energy, environmental and economic points of views were determined among $3 \times 3 \times 3 = 27$ simulations. Giordano et Raymond studied a solar BTES in artic conditions with TRNSYS, comparing five sets of parameters and deriving costs and CO_2 content [25,26]. Veyron et al. the exergoeconomic impact of the integration of a BTES in an existing 3rd generation district heating [27].

Panno et al. reported a higher efficiency of their solar BTES when the HP evaporator was connected to the STC [20]. This raises the question of how to connect the HP, BTES and STC in a convenient way. Leaving apart the BTES, and based on a comprehensive review, Fan et al. recently reported four challenges faced by solar assisted HP [28], namely: (i) poor energy performance at low ambient temperatures; (ii) difficulty in coupling solar thermal collectors with heat pumps to achieve increased operational time and reduced electrical energy usage; (iii) mismatch between heat demand of the building and heat supply of the solar assisted HP; and (iv) lack of multi-functional modelling tool. According to Fan et al., point (i) could be tackled by coupling the HP to long-term thermal storages. Emmi et al. performed an analysis of solar assisted ground source heat pumps in cold climates [29]. However they did not consider solar direct heating or direct discharge from the BTES nor the DHW requirement.

Therefore, to our knowledge, a general system combining Solar Thermal Collectors and Borehole Thermal Energy Storage for space heating and Domestic Hot Water, through a Heap Pump or directly (bypassing the HP) has not been already described. Qualitatively, the combination of the three subsystems (STC, BTES and HP) should allow

Table 1
Building and climate parameters.

Minimum outside air temperature $T_{air,min}$ [°C]	−3.41
Set point for building internal temperature $T_{sp,\ building}$ [°C]	19.0
Building surficial heat loss coefficient G_s [W.m^{-2}.K^{-1}]	1.116
Building surface $S_{building}$ [m^2]	10 000
Outside air temperature allowing heating cutoff T_{cutoff} [°C]	16.0

to reach higher fractions of renewable heat than the combination of one or two subsystems. The expected synergies between the subsystems are as follows:

- The BTES can store the summer excess heat from the STC, at a time where the STC temperature can reach high, critical values. This will lower the summer STC operating temperature which. This, in turn, allows the installation of larger surface of STC to cover the thermal needs in winter and mid-season.
- The presence of an HP is expected to dramatically increase the amount of thermal energy retrieved from the BTES and STC, since it makes energy with temperatures below the desired setpoint available. The HP will however consume a little amount of electricity to do so.

This paper introduces the design of such a multi-source system, including in-depth description of the components, their integration and the control strategy (section 2). The energy flux balances are evaluated for a baseline scenario (section 3). The system is compared to three alternative designs in section 4.1 and one-at-a-time sensitivity analysis is reported in section 4.2. The system optimization is out of the scope of this paper, and multi-objective optimization through surrogate modelling will be reported later.

2. Materials and methods

2.1. Thermal energy requirement

We considered a 10 000 m^2 (floor area) multi-apartment building located close to Paris, France, corresponding to H1a zone of the French thermal regulation RT2012 (see Table 1). This regulation provides hourly climatic data used in this work [30], namely the outside air temperature T_{air}, the tap water temperature $T_{tap\ water}$ to be warmed up for DHW production, the direct normal beam radiation and diffuse radiation on a horizontal surface (cf. Fig. 1). The building is characterized by a heat loss coefficient G_s [W.m^{-2}.K^{-1}] and the heating demand $P_{heating}$ [W] is expressed as:

$$P_{heating} = \begin{cases} G_s \times S_{building} \times \left(T_{cutoff} - T_{air}\right) & \text{if } T_{air} < T_{cutoff} \\ 0 \quad \text{otherwise} \end{cases} \quad (1)$$

Further, $P_{heating}$ is set to 0 between the 16th of May and 14th of October. The resulting heating peak power is $P_{heating,max} = 250$ kW and the consumption is $E_{heating} = 510.5$ MWh.y^{-1} (cf. Fig. 2a), i.e. full-load operation duration $t_{eq,heating} = E_{heating}/P_{heating,max} = 2042$ h. Note that dynamic thermal simulations of old, poorly insulated residential buildings in Turin, Italy (similar to Paris climate) reported similarly $t_{heating} = 1676$ h [31]. The set points for departure temperature into the heat emitters $T_{sp,heat}$ changes linearly with the outside air temperature (cf. Fig. 2b). The baseline scenario considers $T_{sp,heat,\ base} = 35$ °C for $T_{air} = -7$ °C, which is relevant for heating floors.

DHW needs were estimated from measurements on a building with 269 "standard housings", i.e. 2-bedrooms apartment of 65 m^2 [32]. The DHW need per standard housing was 125 L.day^{-1} at 40 °C, or $\dot{m}_{DHW} = 802.0$ kg h^{-1} for our 10′000 m^2 building (assuming a water density $\rho_w = 1000$ kg m^{-3}). Coefficients are given to modulate this average value based on the hour, day and month (cf. Annex 1). The energy required to

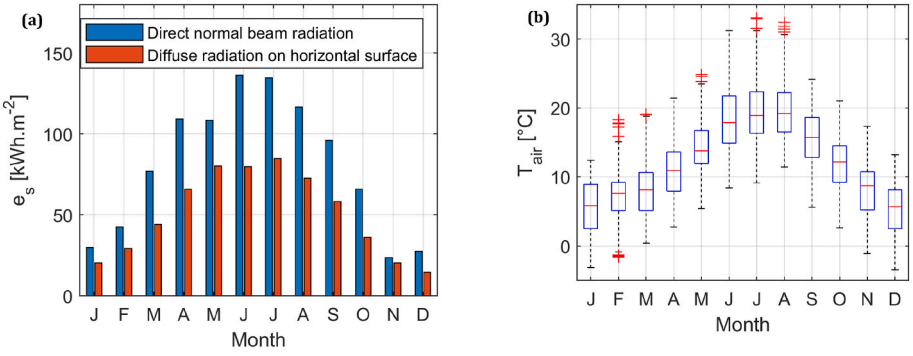

Fig. 1. Climatic conditions: (a) Monthly incoming solar radiations, (b) monthly distributions of the air temperature (The central mark indicates the median, and the bottom and top edges of the box indicate the 25th and 75th percentiles, respectively. The whiskers extend to the most extreme data points not considered outliers, and the outliers are plotted individually using the '+' marker symbol).

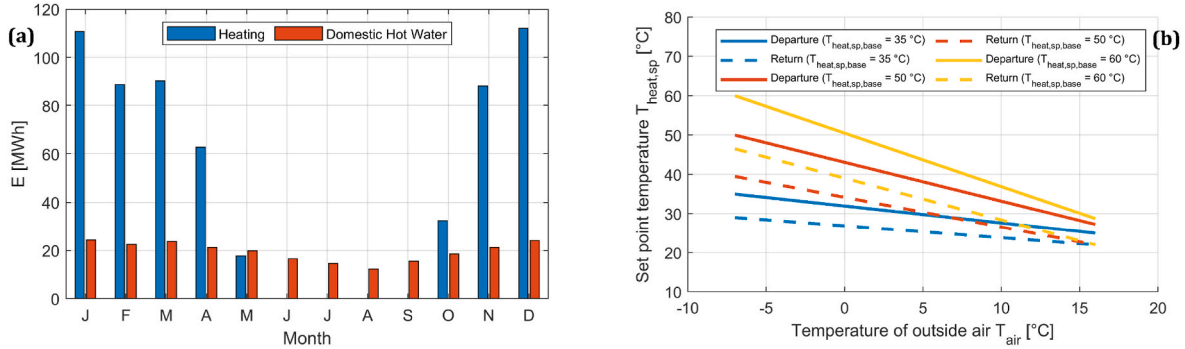

Fig. 2. (a) Monthly heating and DHW needs. (b) Three examples of heating set point temperature as a function of the outside air temperature.

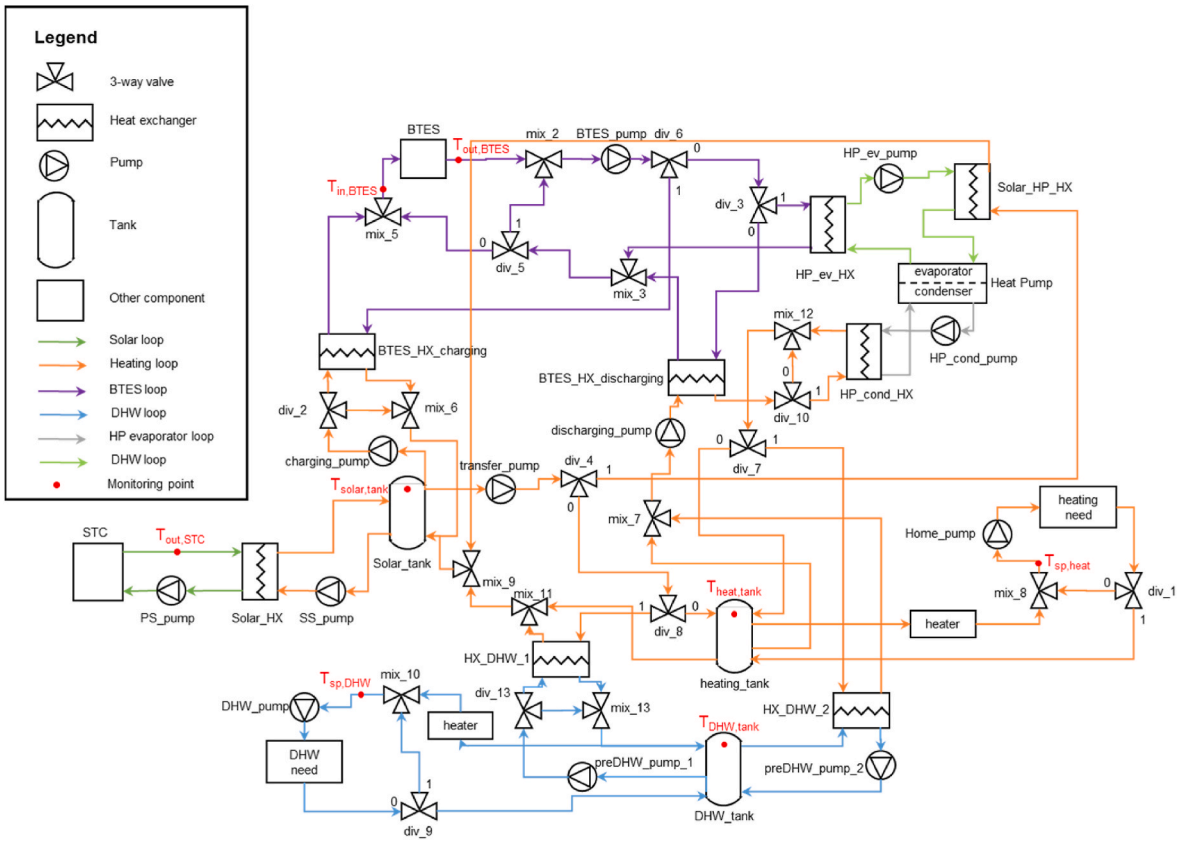

Fig. 3. Hydraulic scheme of the system. The location of the tank inlets and outlets (top or bottom) fits the reality. "0" or "1" on a diverter indicates the fluid output depending on the input signal.

warm up the tap water from its delivery temperature to 40 °C is 226.7 MWh.y^{-1}. DHW reaches about half of the heating need, and is far from being negligible. Cooling requirements are not considered in this study.

2.2. System overview

The designed system encompasses the main subsystems (cf. Fig. 3).

- Solar Thermal Collectors and a solar tank,
- A Borehole Thermal Energy Storage,
- A Heat Pump,
- Distribution loops for heating and Domestic Hot Water, with dedicated tanks and backups.

Additionally the system has hydraulic organs such as three-way valves (diverters and mixers), pumps, heat exchangers and additional tanks. The system is able to transfer solar heat from the solar tank into the BTES. It provides heat to the building through height possible modes: supply of space heating or DHW, from the STC or from the BTES, directly or through the HP. This results in $1 + 2 \times 2 \times 2 = 9$ possible modes of operation (cf. Fig. 4).

2.3. System modelling

The system is modelled in TRNSYS [11] with a time step of $\Delta t = 7.5$ min over 7 years. The integration and convergence tolerances are set to 10^{-3}. To ensure reliable results, the number of time steps without convergence could not exceed 100 without throwing an error. Because of this restrictive setting, the allowed number of iterations per time step was set to a very high value (20 000). MATLAB® [33] is used to prepare and call the deck files (text files describing the model), post-process TRNSYS output files and to perform the sensitivity analysis.

2.4. Components

2.4.1. Heating distribution

A backup heater (Type 138) downstream the heating tank ensures that the set point $T_{sp,heat}$ is met in case the heating tank is not warm enough. The valves *div_1/mix_8* recirculate cooled fluid flowing back from the building if the tank is too warm to meet the set point.

2.4.2. Domestic Hot Water distribution

The DHW is stored in a tank whose volume is expressed as:

$$V_{DHW} = \frac{t_{DHW}\dot{m}_{DHW}}{\rho_w} \quad (2)$$

With $t_{DHW} = 2$ h for the baseline scenario. The tank collects heat from the solar tank and the condenser HP via two dedicated exchangers, respectively *HX_DHW_1* and *HX_DHW_2*. Note that a more common option would be to use immerged heat exchangers in the tank, but the accurate sizing of such exchangers requires many semi-empirical parameters to be determined (typically 8–10), which is out of the scope of this study. Downstream the tank, the valves *div_9* and *mix_10* controlled by a Type 115 ensures that the DHW temperature of distribution does not exceed the distribution set point $T_{sp,DHW} = 40$ °C, a typical value for DHW use, mixing hot fluid with some cool tap water if needed. An external backup heater may warm the water leaving the DHW tank (if too cold) to reach $T_{sp,DHW}$.

The French regulation enforces operational constraints for any storage exceeding 400 L so that to avoid the development of legionella: (i) either the DHW is distributed at 55 °C, or at least every 24 h the tank temperature must reach (ii) 70 °C for 2 min, (iii) 65 °C for 4 min or (iv) 60 °C for 60 min [34]. The option (iii) was chosen here. Every morning at 5 a.m., the model checks if the temperature at the bottom of the tank

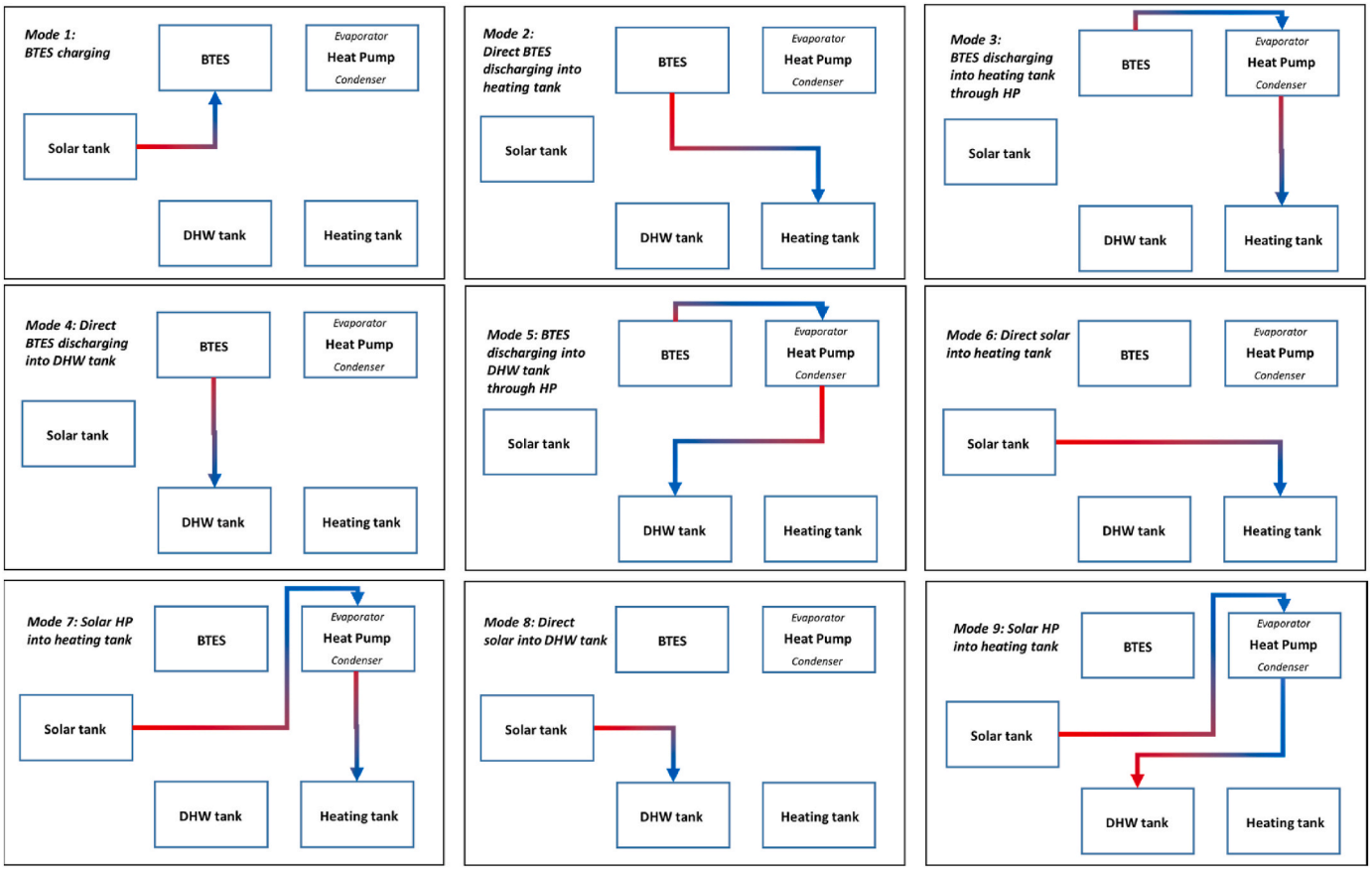

Fig. 4. Functional view of the system.

Table 2
Parameters for the STC and BTES models in TRNSYS.

Solar Thermal Collectors (Type 1346)		Borehole Thermal Energy Storage (Type 557b)	
Intercept efficiency a_0 [-]	0.814	Storage volume [m^3]	15000
Efficiency slope a_1 [$W.m^{-2}.K^{-1}$]	4.81	Borehole depth [m]	35
Efficiency curvature a_2 [$W.m^{-2}.K^{-2}$]	0.0230	Spacing between adjacent boreholes d_{BHE} [m]	3
Tested flow rate [$kg.h^{-1}.m^{-2}$]	76.8	Area of the storage volume S_{BTES} [m^2]	874.0
Surface S_{STC} [m^2]	2500	Radius of the storage r_{BTES} [m]	11.7
1st order Incidence Angle Modifier (IAM) [a]	0.89	Number of boreholes N_{BHE} [−]	55
2nd order IAM [a]	0	Number of boreholes in series [−]	3
		Borehole resistance R_b [$K.m.W^{-1}$]	0.07
		Thickness of the insulation layer e_{insul} [m]	0
		Insulation thermal conductivity λ_{insul} [$W.K^{-1}.m^{-1}$]	0.03
		Extension of the insulation beyond the BTES volume ℓ_{insul} [m]	5
		Initial temperature T_0 [°C]	12
		Storage thermal conductivity λ_m [$W.K^{-1}.m^{-1}$]	2.0
		Storage heat capacity $(\rho C_p)_m$ [$MJ.K^{-1}.m^{-3}$]	2.2

[a] See TRNSYS manual.

(where the cold tap water enters) reached $T_{boost\ DHW} = 65\ °C$ at least once in the past 24 h. If not, the tank is warmed up. The power P_i is applied to every node i of the tank:

$$P_i = \frac{(\rho C_p)_w \times V_{DHW} \times (T_{boost\ DHW} - T_i)}{10 \times \Delta t} \quad (1 \le i \le 10) \tag{3}$$

This results in a total power $P_{boost\ DHW} = \sum_{i=1}^{10} P_i$.

2.4.3. Solar thermal collectors (STC) and solar tank

The STC are modelled with the Type 1346. The STC efficiency η_{STC} is computed as:

$$\eta_{STC} = \frac{P}{\varphi_{rad} S} = a_0 - a_1 \frac{T_{in} - T_{amb}}{\varphi_{rad}} - a_2 \left(\frac{T_{in} - T_{amb}}{\varphi_{rad}} \right)^2 \tag{4}$$

Where,

- P: thermal power delivered by the STC [W]
- φ_{rad}: incoming solar radiation on the STC [$W.m^{-2}$]
- T_{in}: inlet temperature [°C]
- T_{amb}: ambiant temperature [°C]
- S: STC surface [m^2]
- a_0, a_1 and a_2 three empirical coefficients

The data originates the technical documentation of VITOSOL 100-FM (plan), type SV1F (cf. Table 2). Note that the RT2012 climatic file provides solar visible radiations as *Direct normal beam radiation* and *Diffuse radiation on horizontal surface*. Type16k was used to convert these to *Incident radiation*, *Total horizontal radiation* and *Horizontal diffuse radiation* as inputs of Type 1346.

The STC outlet fluid enters the solar tank by its top and the charging and transfer pumps are fed from the top of the solar tank. The heat transfer from the STC to the solar tank is controlled by a differential

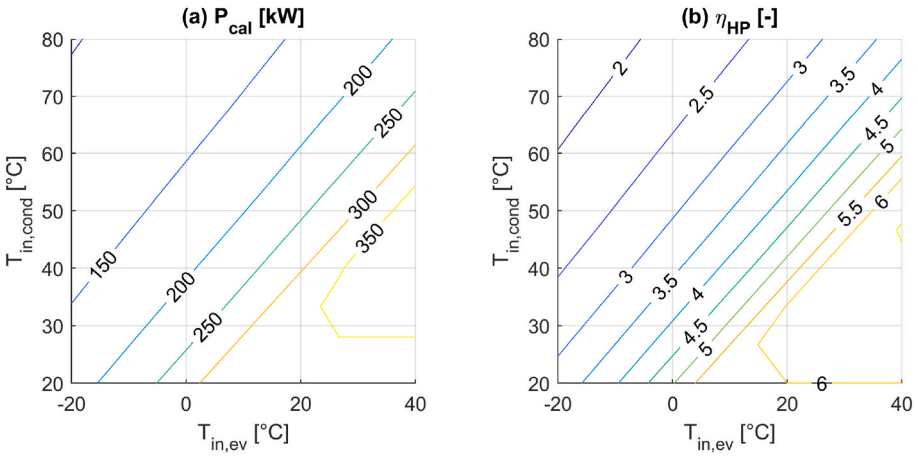

Fig. 5. Characteristics of the HP as a function of evaporator and condenser inlet temperatures $T_{in,ev}$ and $T_{in,cond}$: (a) calorific power, (b) Coefficient Of Performance.

Table 3
Parameters of the TRNSYS tanks.

	Number of ports	Volume [m^3]
Solar tank	3	100.00
Heating tank	3	14.00
DHW_tank	3	1.66

Table 4
Parameters of the TRNSYS pumps.

	Variable speed?	Rated power [kW]
PS_pump	No	6.94
SS_pump	No	1.39
charging_pump	No	4.67
discharging_pump	No	4.67

controller (Type 165). It compares the temperatures of the STC to solar tank and starts *PS_pump* and *SS_pump* as soon as the difference is higher than 2 °C, and stops when the difference reaches 0 °C.

2.4.4. Borehole Thermal Energy Storage

The BTES was modelled with Duct Storage (DST, Type 557), which considers heat transfer by conduction only, and was validated against Neckarsulm BTES [7]. The initial ground temperature and ground thermal conductivity are representative of surficial formations of Paris basin [35,36]. Note that in the baseline scenario the uppermost surface of the BTES is not insulated. In Table 2, the area of the storage volume S_{BTES} is computed as:

$$S_{BTES} = \pi (r_{BTES} + \ell_{insul})^2_{=\pi} \left(\sqrt{\frac{V_{BTES}}{\pi H_{BHE}}} + \ell_{insul} \right)^2 \quad (5)$$

While the number of BHE is computed as:

$$N_{BHE} = \text{ceil}\left(\frac{2}{\sqrt{3}} \frac{V_{BTES}}{{d_{BHE}}^2 H_{BHE}} \right) \quad (6)$$

2.4.5. Heat pump (HP)

The HP is modelled by Type 927 with a nominal calorific power set to 250 kW for $T_{out,ev} = 0$ °C and $T_{out,\ cond} = 35$ °C. The compressor electrical consumption is kept constant throughout the whole domain at $P_{elec,ref} =$ 56.79 kW. The performance maps (Fig. 5) required by Type 927 are derived from CIAT manufacturer datasheets (cf. and Annex 2 for further details). The condenser is connected to a dedicated heat exchanger HP_cond_HX. The evaporator is connected to the BTES through HP_ev_HX and to the solar tank through solar_HP_HX. These heat exchangers decouple the HP source (BTES or solar) from the distribution (heating or DHW).

2.4.6. Tanks

All tanks are modelled with Type 534 (see Table 3). Tanks are divided into 10 vertical nodes. Warm fluid always enters the tank by its top (node #2), and conversely cool fluid enters by the bottom of the tank (node #9), as represented in Fig. 3. The tanks are recovered with 10 cm of an insulation material ($\lambda = 0.03$ W.K^{-1} m^{-1}). Accounting for a convective transfer coefficient of 0.11 W.K^{-1} m^{-2}, this results in a heat transfer coefficient $h = 1/(0{,}11 + 0{,}1/0{,}03) = 0.29$ W.K^{-1} m^{-2}. The temperatures on all outer faces of the tanks is assumed to be 20 °C.

2.4.7. Pumps

All pumps are On/Off pumps (modelled by Type 114), except the DHW and heating pumps (modelled by Type 110), see Table 4. The electric consumption of the distribution pumps (home_pump, DHW_pump, preDHW_pump_1 and preDHW_pump_2) is not included in the analysis.

2.4.8. Heat exchangers

Heat exchangers reported in Table 5 are counter-flow exchangers, modelled with Type 5. The heat transfer coefficients k were computed with the NUT-ε method [37] to ensure a pinch $\Delta T = 2$ °C under the "nominal conditions" defined in Table 5 (see Annex 3 for further details). HP_cond_HX, HP_ev_HX and solar_HP _HX are assumed to have constant thermal efficiencies $\eta = 85\%$.

2.5. System control

The core of the system is controlled by a microprocessor. A microprocessor performs logical comparisons between system variables to set a status to actuators. It uses a status array to determine in which mode it should operate, and an output array to determine the actuators states in each mode. Dead bands ensure hysteresis and prevent the controller from switching from mode to mode too often. TRNSYS provides a microprocessor (Type 40), but a limitation of five comparators is hard-coded. The Fortran source code was modified to increase this limit and allow both status and output arrays to be given as external text files, gaining in convenience. The subsequent rebuilt Type 40 was validated against the example provided with TRNSYS documentation, yielding exactly the same results.

The control strategy was designed with the following considerations in mind:

Table 5
Nominal conditions for the heat exchangers sizing. $C_{p,c}$, $\dot{m}_c$, $T_{in,c}$, $C_{p,h}$, $\dot{m}_h$, $T_{in,h}$ are the fluid specific heats, mass-flow rates, and inlet temperatures at the cold and hot sides respectively.

	$\dot{m}_h$ [kg.s^{-1}]	$\dot{m}_c$ [kg.s^{-1}]	$T_{in,h}$ [°C]	$T_{in,c}$ [°C]	$C_{p,h}$ [J.K^{-1}.kg^{-1}]	$C_{p,c}$ [J.K^{-1}.kg^{-1}]	k [kW.K^{-1}]
Solar_HX	17.36	17.36	80	40	3795	4180	723.6
BTES_HX_charging	15.65	15.65	70	40	4180	3795	883.1
BTES_HX_2	15.65	15.65	60	35	4180	4180	730.1
HX_DHW_1	11.67	11.67	40	25	4180	4180	317.0
HX_DHW_2	11.67	11.67	40	25	4180	4180	317.0

(i) The solar heat can be transferred to the BTES only if the distribution and DHW tanks are already at their desired set points. Heat can be stored into the BTES at any time in the year, even in winter, but one should avoid transferring some solar heat into the BTES that may be useful a few hours later for DHW or heating.
(ii) If the temperature of both the heating and DHW tanks are below their respective set points, then the system feeds the heating tank as a priority.
(iii) If one tank must be filled, the source (solar tank or BTES) with the highest temperature is selected.
(iv) This source must be used directly as long as its temperature is higher than the desired set point, otherwise the source feeds the HP evaporator while the tank is warmed up by the HP condenser.

The system can operate in nine modes (see Annex 4). Mode 1 transfers the excess of solar heat into the BTES, while modes 2 to 9 produces space heating and DHW. The mode is selected based on the states of 10 comparators Ci:

- C2 and C5 compare the temperature of the DHW and heating tanks to their respective set points;
- C1 and C4 compare the solar tank temperatures to the DHW and heating set points;
- C7 and C8 acts similarly, except it considers the BTES outlet instead of the solar tank;
- C6 compares the solar tank temperature to the BTES outlet temperature and is involved in determining if solar heat can be transferred into the BTES. C2 compares the same quantities, but is involved in selecting the "best" source when thermal energy is needed.
- C9 compares the BTES outlet temperature to a criteria $T_{out,\ BTES,min} = 8$ °C. It is used to shut the system down if the BTES fluid temperature gets too low. C10 operates similarly for the solar tank.

To improve the model convergence, the inputs of the comparators are delayed by one time step. The mods act as follow.

- **Mode 1: BTES charging:** the charging pump is ON and the valve *div_6* is in position 1. This ensures that the HP tank and the direct discharge exchanger *BTES_HX_2* are bypassed. Regulations may impose a limitation on the BTES inlet temperature. For instance, in France, a 40 °C threshold is a condition to benefit for a simplified regulatory regime. The BTES outlet fluid flows directly to the charging exchanger, while *div_2* ensures that some fluid is mixed with the warmed fluid exiting this exchanger to ensure the maximal charging temperature criteria is met. Such limitation was not enforced in the baseline scenario. This mode is activated if both heating and DHW tanks are above their set points, and the solar tank is warmer than the BTES outlet temperature.
- **Mode 2: Direct BTES heating (no HP):** the discharging pump is ON, liquid exiting the heating tank is warmed up by *BTES_HX_2*. *div_3* and *div_6* are in position 0, which ensures that the BTES outlet is connected to *BTES_HX_2* and the HP is bypassed. This mode is activated if the heating tank temperature is below its set point, and the BTES outlet is warmer than both the solar and heating tank set point.
- **Mode 3: BTES heating through HP:** the discharging pump is ON. The HP and the evaporator pump *HP_ev_pump* are in position 1, as *div_3*, ensuring that the BTES outlet bypasses *BTES_HX_2*. The same conditions applies as for mode 2, except that the BTES outlet must be cooler than the heating tank.
- **Mode 4: Direct BTES DHW (no HP):** Operates as mode 2, unless the valves *div_7* and *div_8* are in position 1 to feed to the DHW tank instead of the heating tank. This mode is activated if the DHW tank temperature is below its set point *and* the heating tank is warmer than its set point (see point (iii) above). Otherwise, the same conditions as mode 2 apply, considering the set point for DHW tank instead of heating tank.
- **Mode 5: BTES DHW through HP:** Operates as mode 3, unless the valves *div_7* and *div_8* are in position 1 for the same reasons as for mode 4. As for mode 4, this is activated if the DHW tank temperature is below its set point *and* the heating tank is warmer than its set point. Otherwise, the same conditions as mode 3 apply, considering the set point for DHW tank instead of heating tank.
- **Mode 6: Direct solar heating:** The transfer pump is ON, warm fluid is transferred from the solar to the heating tank. The heating tank must be below its set point, while the solar tank must be warmer than the heating tank set point, the BTES outlet temperature.
- **Mode 7: Solar heating trough HP:** The transfer pump is ON, while *div_4* is in position 1, which feeds *solar_HP_HX* is fed. The discharging pump is on to collect heat from the HP condenser and transfer it back to the heating tank. So does the HP, HP_ev_pump and div_3. Note that the position of div_3 is of no consequence since div_6 is in position 1, therefore the BTES outlet fluid bypasses both *HP_tank* and *BTES_HX_2*. The heating tank temperature must be below its set point. The solar tank temperature is below the heating set point and above the BTES outlet temperature, which justifies the use of the solar HP.
- **Mode 8: Direct solar DHW:** Operates as mode 6, unless the valves *div_7* and *div_8* are in position 1 to feed the DHW tank. As for mode 4, the DHW tank temperature must be below its set point *and* the heating tank above its set point. The solar tank is warmer than the BTES outlet (and therefore is a better source), and warmer than DHW tank set point.
- **Mode 9: Solar DHW through HP:** Operates as mode 7, unless the valves *div_7* and *div_8* are in position 1. As for mode 8, is activated if the DHW tank is below its set point. As for mode 7, the solar tank temperature is below the heating set point and above the BTES outlet temperature, which justifies the use of the solar HP.

The HP power must be modulated to prevent undercooling the heat sink or overheating the heat source during one time step. The modulation factors for DHW production is defined as:

$$f_{HP,DHW} = \min\left(\frac{(\rho C_p)_w\, V_{DHW}\, \Delta T_{DHW,HP}}{\Delta t\, P_{cal\ HP}}, 1\right) = 0.248 \tag{7}$$

With $\Delta T_{DHW,HP} = 5$ °C, for HP fed by the solar tank:

$$f_{HP,sol} = \min\left(\frac{(\rho C_p)_w\, V_{sol}\, \Delta T_{sol,HP}}{\Delta t\, P_{fr\ HP}}, 1\right) = 1 \tag{8}$$

Table 6
Summary of alternative designs, including operation modes and the normalized amount of electricity and backup needed to produce thermal energy.

System	Heat pump	BTES	Possible operation modes	E_{ext}^*	$E_{ext,w/o\ pumps}^*$
A	No	No	6, 8	0.612	0.603
B	Yes	Yes	6, 7, 8, 9	0.480	0.461
C	No	Yes	1, 2, 4, 6, 8	0.591	0.548
D	Yes	Yes	1–9	0.274	0.216

With $\Delta T_{sol,HP} = 5\ °C$ and $P_{fr\ HP} = 197$ kW the nominal frigorific power of the HP. For HP fed by the BTES:

$$f_{HP,BTES} = \min\left(\frac{p_{lin} L_{BHE}}{P_{fr\ HP}}, 1\right) = 0.567 \tag{9}$$

With $p_{lin} = 70\ \mathrm{W\ m^{-1}}$, a typical ratio of power applied per meter of BHE [43]. For every mode with a HP, the HP power must be modulated by the worst factor. This lead to the following modulations:

$$\begin{aligned}
&\text{Mode 3}: f_{HP\ mode\ 3} = f_{HP,BTES} = 0.567\\
&\text{Mode 5}: f_{HP\ mode\ 5} = \min\left(f_{HP,BTES}, f_{HP,DHW}\right) = 0.248\\
&\text{Mode 7}: f_{HP\ mode\ 7} = f_{HP,sol} = 1\\
&\text{Mode 9}: f_{HP\ mode\ 9} = \min\left(f_{HP,sol}, f_{HP,DHW}\right) = 0.248
\end{aligned} \tag{10}$$

The flow-rates in pumps HP_ev_pump and HP_cond_pump are scaled accordingly.

Note that more advanced strategies have been proposed for UTES control, including a servo-controller [38], an agent-based controller [39] or a model-based predictive controller [40]. The latter was numerically tested with Solar Drake Landing and was found to outperform conventional differential controllers when minimizing the electricity consumptions of the pumps.

2.6. Alternative designs

The system is compared to three alternatives designs, each design containing only a fraction of the three main components (cf. Table 6). For convenience, the TRNSYS models keep all components, the control strategy ensuring the selection of the appropriate operation modes. In alternative designs *A* and *C*, the lower inputs #4 and #8 of the microprocessor are fed with $T_{tap,\ water}$ instead of $T_{tank,DHW}$: Since there is no HP, the solar tank will heat the DHW even though it does not reach the desired set point to save backup. Since alternative designs A and B have no BTES, a fake temperature of −10 °C is sent to lower input #3 to ensure the microprocessor does not select the BTES.

2.7. Qualitative verification of the model

For each simulation reported in this paper, the qualitative behavior of the system is verified by checking the monthly heat balances of heating, DHW and solar productions (cf. Fig. 6), reading respectively:

$$\begin{aligned}
E_{heating} + E_{heating\ tank\ loss} = {} & E_{dir,sol,heating} + E_{frig,sol,heating} + E_{el,sol,heating}\\
& + E_{dir,BTES,heating} + E_{frig,BTES,heating} + E_{el,BTES,heating}\\
& + E_{backup,heating}
\end{aligned} \tag{11}$$

$$\begin{aligned}
E_{DHW} + E_{DHW\ tank\ loss} = {} & E_{dir,sol,DHW} + E_{frig,sol,DHW} + E_{el,sol,DHW} + E_{dir,BTES,DHW}\\
& + E_{frig,BTES,DHW} + E_{el,BTES,DHW} + E_{backup,DHW}\\
& + E_{boost,DHW}
\end{aligned} \tag{12}$$

$$E_{coll\ solar} + E_{solar\ tank\ loss} = E_{dir,sol,DHW} + E_{frig,sol,DHW} + E_{load,BTES} + E_{int\ solar\ tank} \tag{13}$$

The solar tank volume V_{sol} cannot be overlooked, eq. (13) accounts for the change in internal energy of the tank $E_{int\ solar\ tank}$:

$$E_{int\ solar\ tank} = \iint \left(\rho C_p\right)_{water} V_{sol} (T - T_0)\ \mathrm{d}V\ \mathrm{d}t \tag{14}$$

To allow comparing the simulation of systems of various sizes, the energy amounts are preferentially normalized as E^*, the ratio of the energy to the total building heat demand:

$$E^* = \frac{E}{E_{heating} + E_{DHW}} \tag{15}$$

3. Results and discussion for the baseline scenario

3.1. Monthly energy mix

Monthly origins of heating and DHW are reported in Fig. 7, along with balances on the solar tank and the BTES. It takes about 4 years to reach a periodic regime, i.e. starting at the 5th year the energy origins will remain the same from one year to the next one. During the 7th year of operation, the solar panels collect 691.3 MWh, 158.5 MWh are used directly (22.9%), 144.5 MWh indirectly (i.e. through the HP, 20.9%) and 393.4 MWh are transferred into the BTES (56.9%), mostly during the summer (cf. Fig. 7a). During the first half of the heating season, the heating tank is mostly fed by the HP on BTES (cf. Fig. 7b). Indeed, the BTES is warm enough to provide direct heating only in October and November. Overall, the extraction from the BTES through the HP

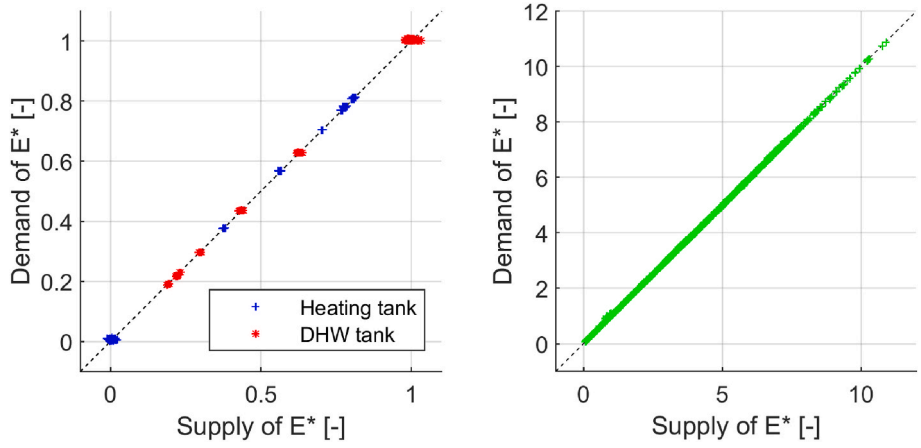

Fig. 6. Heat balance on (a) the heating and DHW tanks and (b) solar tank on a monthly basis, making up 12000 monthly values. "Supply" refers to the left part of eq. 11–13 and "Demand" to the right side.

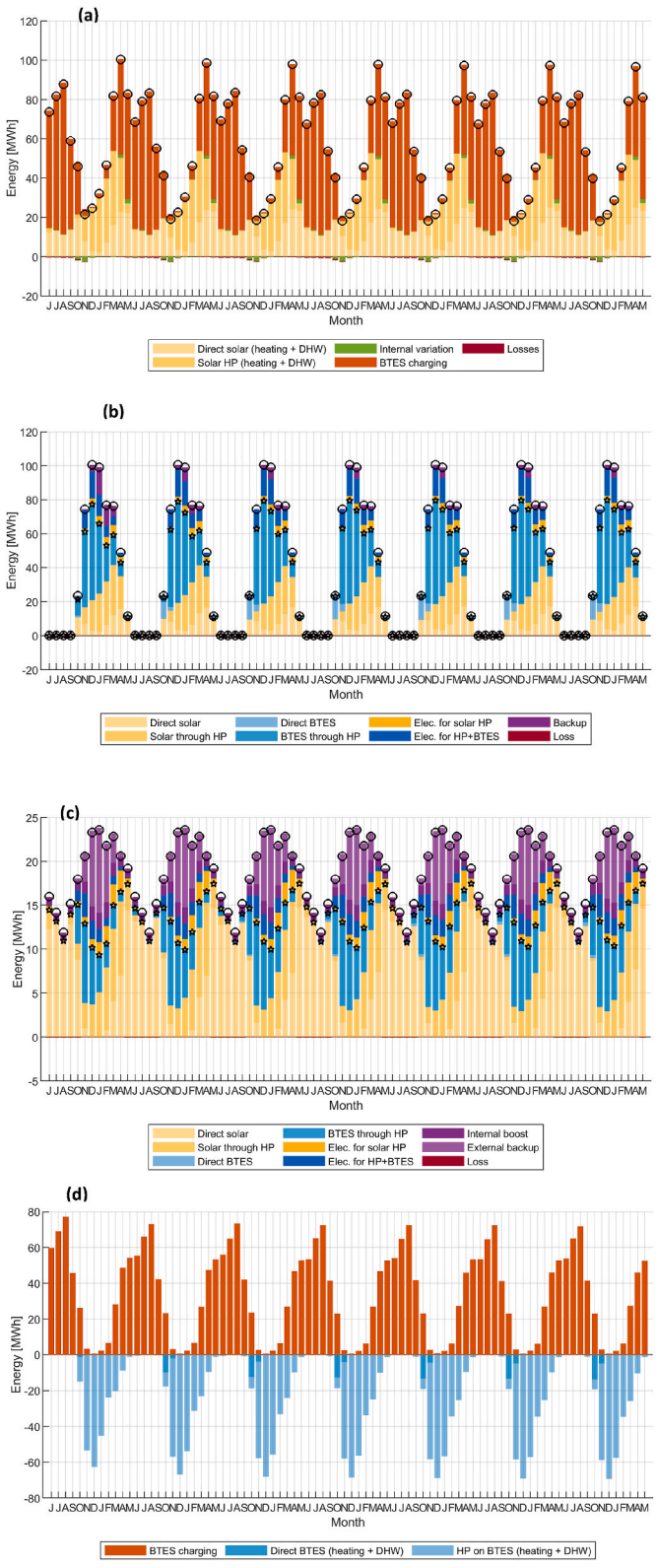

Fig. 7. Baseline scenario: Monthly heat productions of (a) solar energy, (b) heating, (c) DHW and (d) heat balance on the BTES. In subplots (a)–(c), the black dots account for the left part of eq. 13–15. In subplots (b) and (c), the black stars accounts for the cumulated solar and underground energy (i.e. not gas or electricity).

accounts for 42.8% of the heating, the extraction of STC through the HP for 22.9%, the direct solar heat for 13.9%, the electricity for the HP on BTES for 11.6%, the electricity for the solar HP for 4.1%, the direct BTES for 3.6% and the backup boiler for 2.5%. A similar behaviour is observed for the DHW (cf. Fig. 7d), the direct solar accounting for 34.4% of the production, followed by the extraction from the BTES through the HP (17.8%), the solar extraction through the HP (15.4%), the external backup (12.5%), the internal backup (6.5%), the electricity used by the HP on BTES (5.3%) or on STC (4.3%) and the direct BTES (0.4%). The injection of solar energy into the BTES reaches 393.4 MWh, only 19.1 MWh is extracted directly while 259.3 MWh is extracted through the HP (cf. Fig. 7d).

3.2. Operation during typical days

During a summer day, the BTES inlet temperature reaches about +60 °C around noon (cf. Fig. 8). The solar tank is large enough to smooth the solar production, allowing the solar heat to be stored day and night into the BTES (mode #1). The microprocessor sporadically chooses mode #8 (direct solar) to prepare DHW. The control strategy maintains the temperature in the upper part of the DHW tank close to its set point, though external backup is sporadically used to reach the set point. Indeed, the value of udb_5 as high as +10 °C (in absolute value) ensures the DHW production is started early enough before the upper part of the DHW tank falls below $T_{sp,DHW}$.

During a typical winter day, the system is able to provide most heating and DHW without backup, mostly through the BTES and HP (modes #3 and #5) (cf. Fig. 9). Heat accumulates in the solar tank and the temperature in the upper part reaches c.a. 20 °C around 4:00 p.m. Similarly to DHW production, $udb_2 = +3$ °C (in absolute value) ensures that the heating tank is warm enough to reach the set point at any time. However, the control strategy fails to maintain the upper part of the DHW tank at 40 °C. This is probably due to the HP power restriction (eq. (7)), the value $\Delta T_{DHW,HP} = 5$ °C being too low to allow the HP to cope with the fast intake of cold tap water. This illustrates how the energy balance is sensitive to the choice of the parameters values used for the controls.

4. Discussion

4.1. Comparison to alternative designs

The designs can be compared via E_{ext}^*, the normalized amount of electricity and backup needed to produce heating and DHW, as reported in Table 6:

$$E_{ext}^* = \frac{E_{el,HP} + E_{backup,DHW} + E_{boost,DHW} + E_{backup,heating+E_{el,pumps}}}{E_{heating} + E_{DHW}} \quad (16)$$

and $E_{ext,w/o\ pumps}^*$ where the electric consumption of the pumps is overlooked:

$$E_{ext,w/o\ pumps}^* = \frac{E_{el,HP} + E_{backup,DHW} + E_{boost,DHW} + E_{backup,heating}}{E_{heating} + E_{DHW}} \quad (17)$$

Both indicators are computed on the 7th year of operation. Design A requires the largest backup and electricity to cover the thermal demand (cf. Fig. 10b and c). It is not surprising, since the system only has STC. Designs adding a HP (design B) or a BTES (design C) to the STC perform better, but are outperformed by the combination of the STC, HP and BTES (design D).

Design D allows to collect 131% more solar energy compared to Design A (cf. Fig. 10a). Designs C and D experience a much lower maximal temperature at the top of the solar tank in summer (c.a. 60–65 °C) compared to designs A and B (c.a. 100–105 °C) due to the evacuation of excess solar heat into the BTES (cf. Fig. 11a). If the BTES is coupled to a HP (design D), the average temperature of the BTES

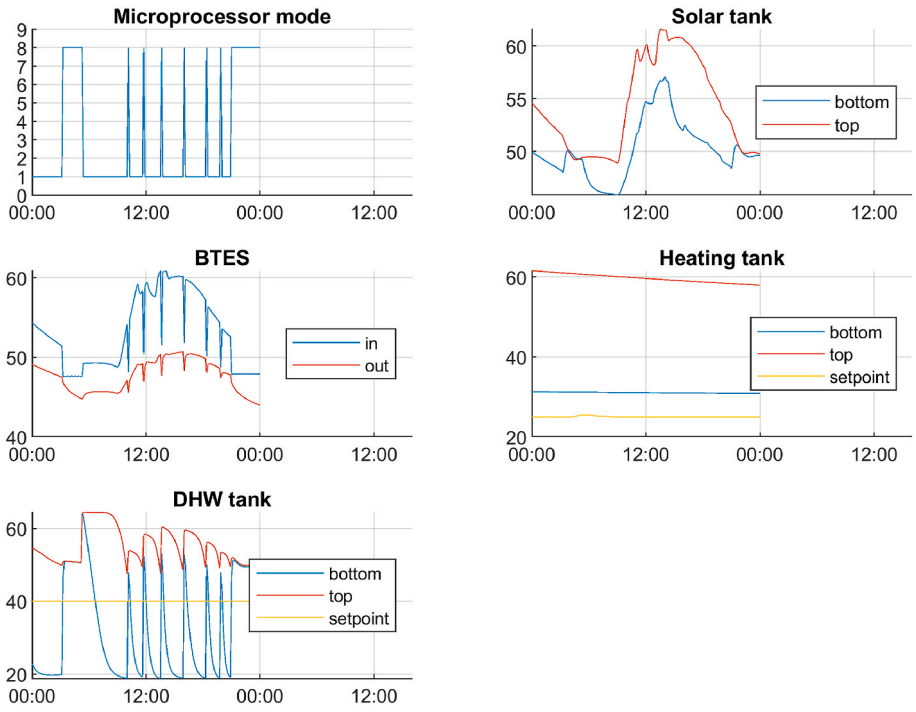

Fig. 8. Baseline scenario: System operation on the 9th of August of the 7th year of simulation, from 00:00am to 23:59pm.

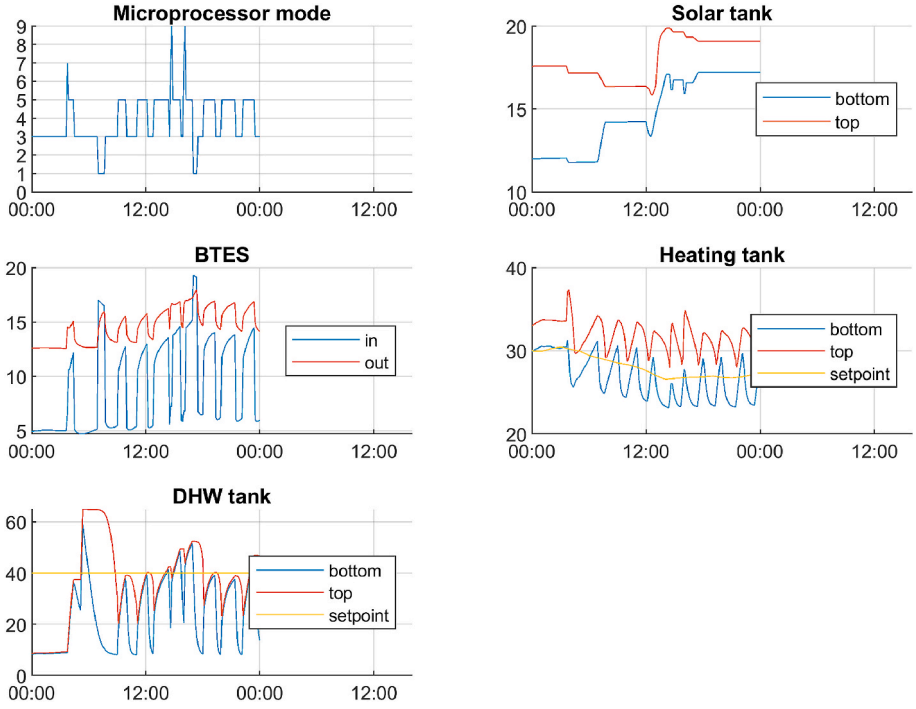

Fig. 9. Baseline scenario: System operation on the 1st of January of the 7th year of simulation.

oscillates between c.a. 42 °C (end of loading in summer) and a low point at c.a. 16 °C in winter (cf. Fig. 11b). The absence of HP (design C) results in a BTES used on a much smaller temperature range (35–50 °C): the BTES cannot be depleted below the heating set point (c.a. 30–35 °C).

4.2. One-at-a-time analysis

Note that when a parameter varies, the heat exchangers are re-sized and the pump electrical consumptions recomputed accordingly to §2.4.7 and §2.4.8.

4.2.1. STC characteristics

The STC area, azimuth and inclination, along with the solar tank volume dramatically affects $E_{ext}{}^{*}$ (cf. Fig. 12). Note that for the investigated parameters, there seems to be an optimal azimuth around $\varphi = 15°$ (i.e. the panel slightly oriented towards the West) and an inclination

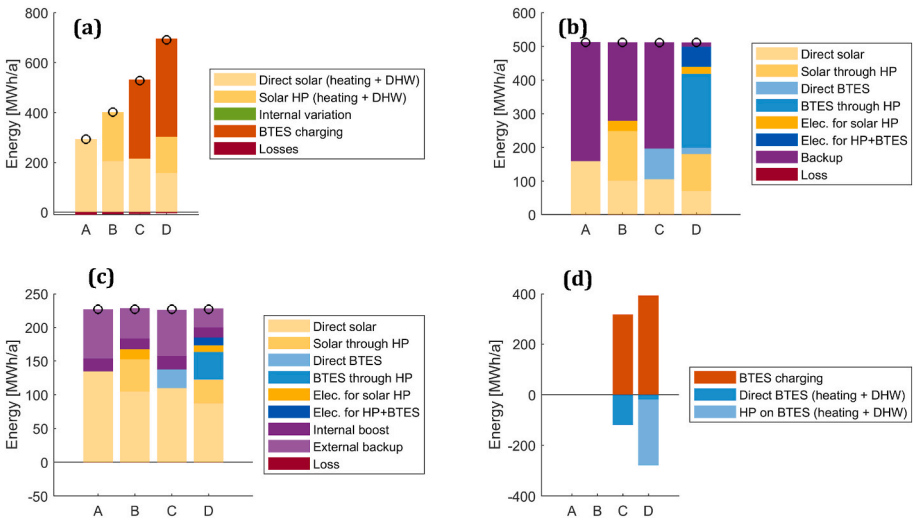

Fig. 10. Comparison of the heat productions of (a) solar energy, (b) heating, (c) DHW and (d) heat balance on BTES for designs A to D, computed on the latest year of operation.

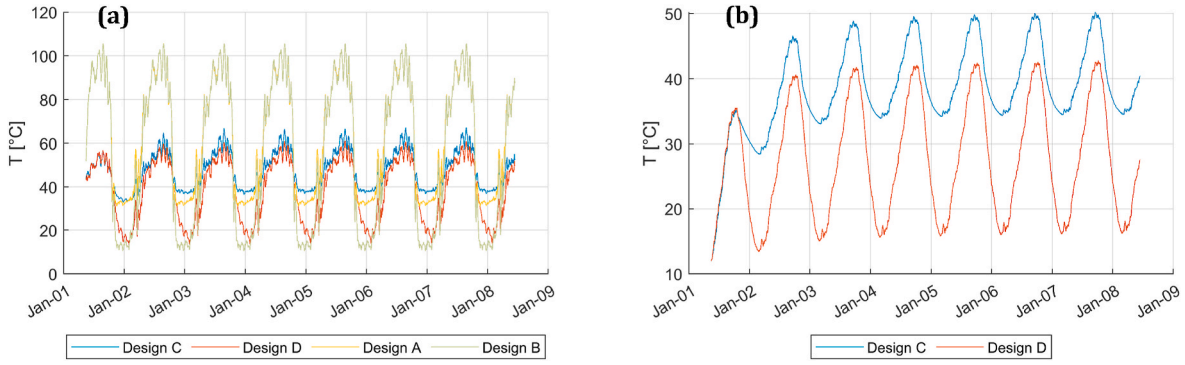

Fig. 11. Evolution of (a) the temperature at the top of the solar tank (after application of a moving mean of 10 days) and (b) the average temperature of the BTES.

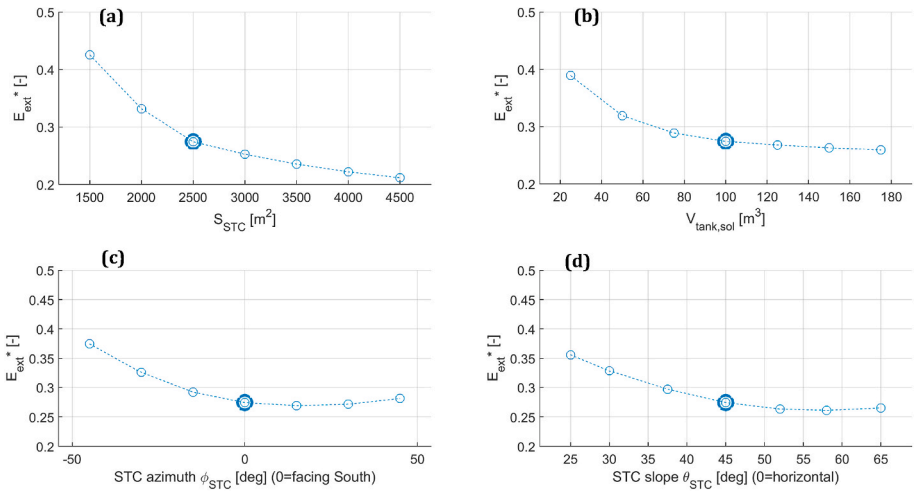

Fig. 12. Influence of STC characteristics. (a) STC area, (b) Solar tank volume, (c) STC azimuth, (d) STC inclination. The bold circle enlightens the baseline scenario.

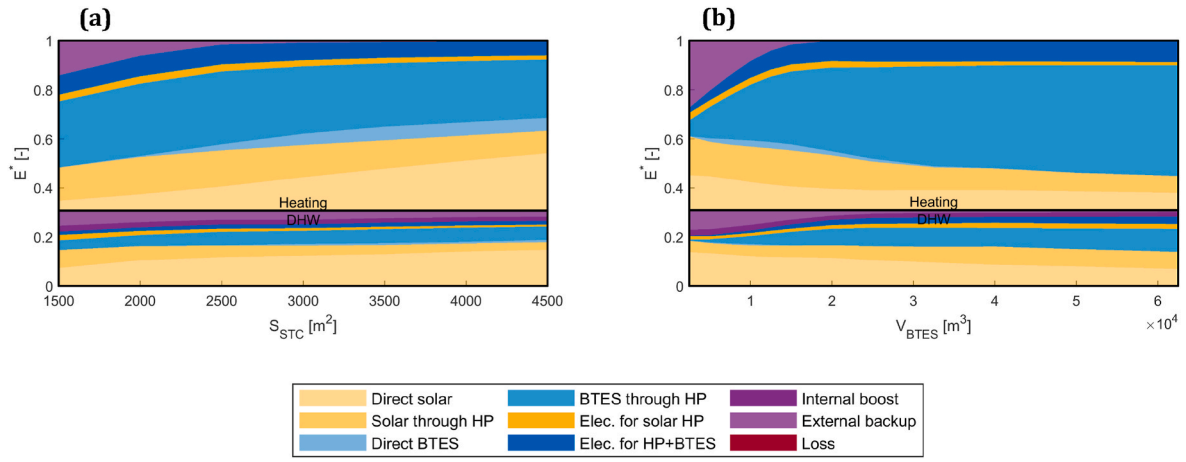

Fig. 13. Cumulative plot of the origin of heating and DHW as a function (a) the STC area, (b) the BTES volume. The lower black rectangle indicates the origin of DHW, the upper one is for heating.

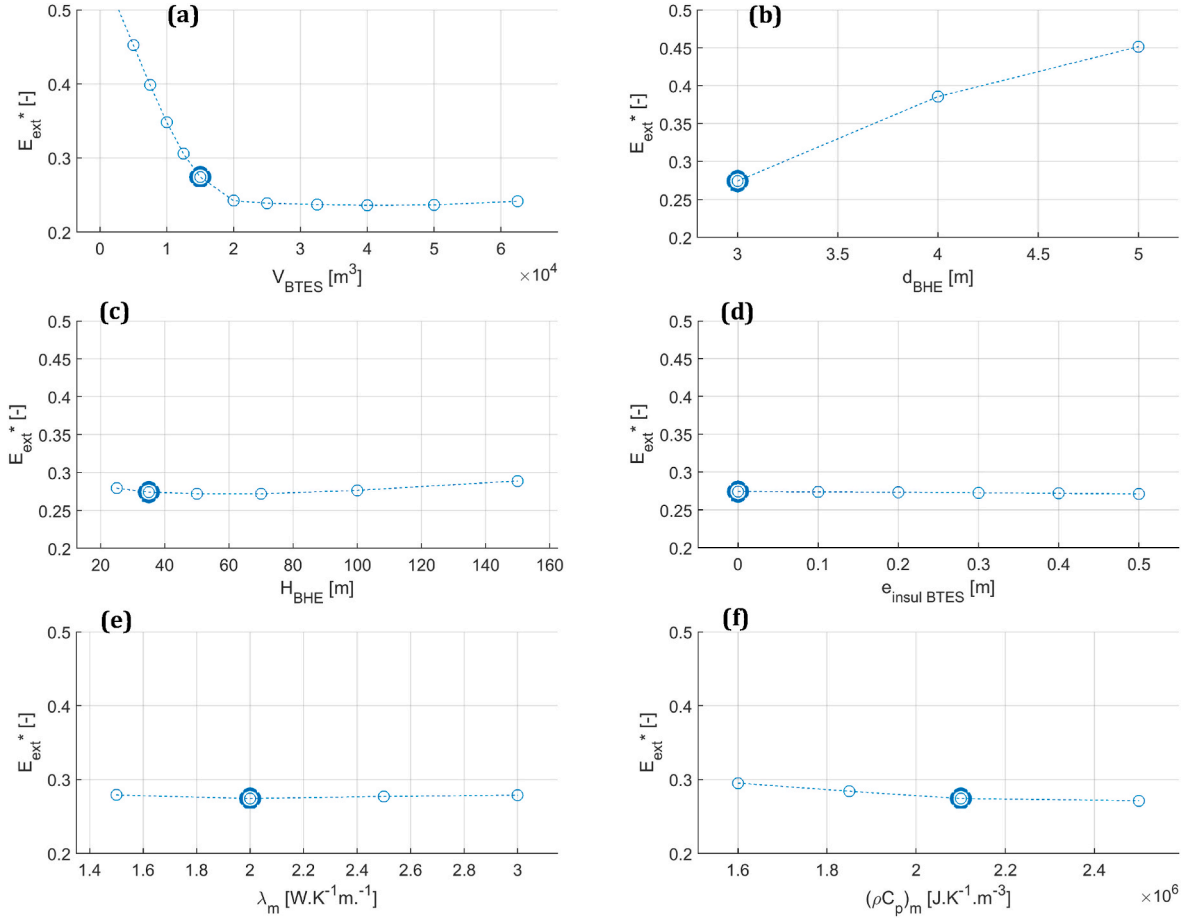

Fig. 14. Influence of BTES characteristics: (a) BTES volume, (b) distance between boreholes, (c) borehole depth (with V_{BTES} and d_{BHE} fixed by the baseline scenario), (d) thickness of insulation, (e) ground thermal conductivity, (f) ground heat capacity.

of $\theta = 57°$. This inclination allows more solar heat to be collected in winter. Increasing the STC area results in more solar heat being used directly, but has a limited influence upon the amount of heat extracted from the BTES (cf. Fig. 13a).

4.2.2. BTES characteristics

Note that the BTES is characterized by its volume V_{BTES}, the borehole depth H_{BHE} and the distance between the boreholes d_{BHE}. The number of boreholes N_{BHE} is computed according to (6), as such it is not an input parameter of the analysis.

The BTES volume and the distance between boreholes have a key influence on $E_{ext}{}^*$ (cf. Fig. 14a and b). Beyond $V_{BTES} = 20000$ m^3, solar heat is stored into the BTES at the expense of the production of solar-sourced thermal energy, resulting in no further increase of the system performance (cf. Fig. 13b).

The influence of the depth is slight, though there seems to be an

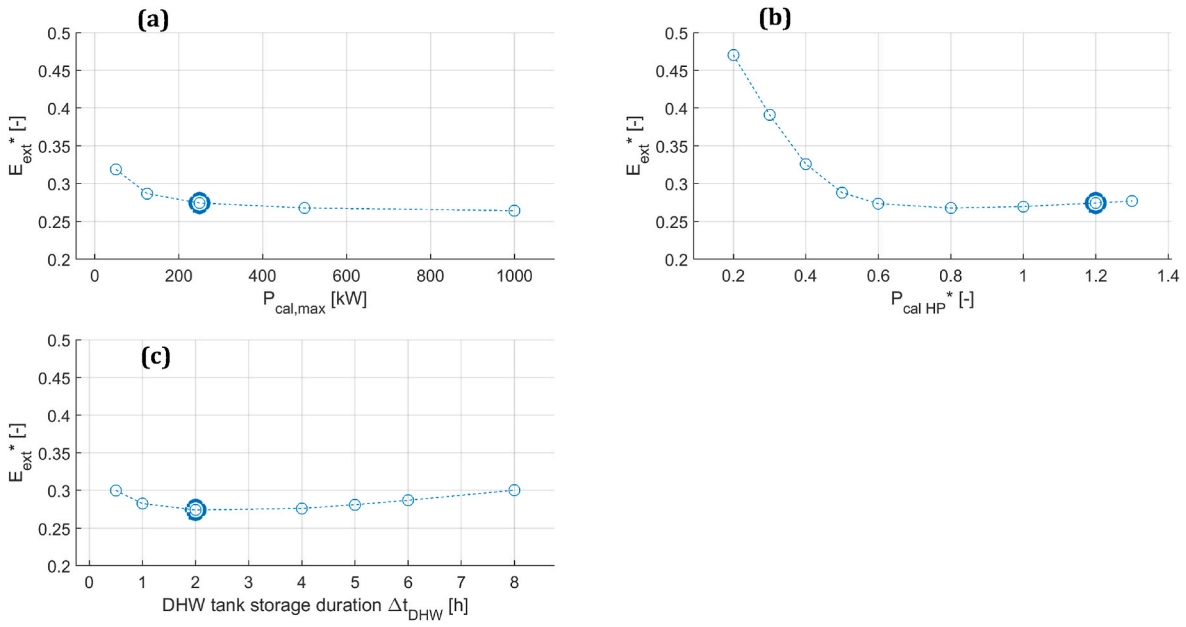

Fig. 15. Influence of Thermal needs characteristics: (a) system size, (b) normalized HP nominal calorific power $P_{cal,HP}^* = P_{cal,HP}/P_{heating,max}$ and (c) nominal storage duration of DHW tank.

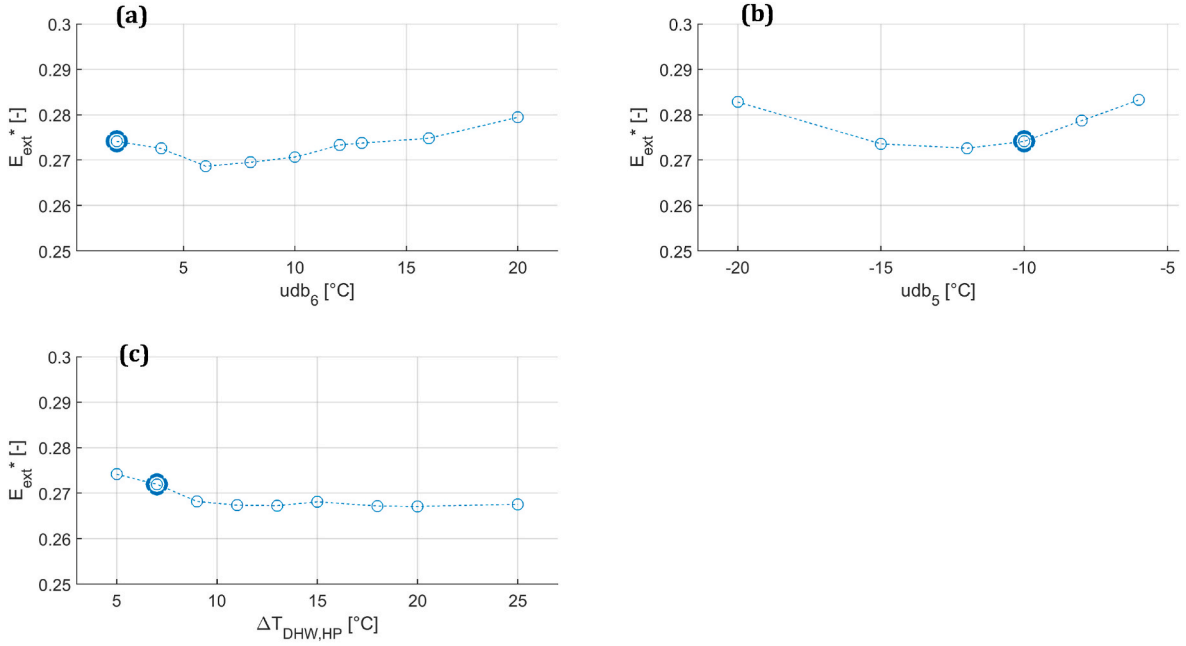

Fig. 16. Influence of 3 parameters of the control strategy (a), upper dead band of comparator #6 (b) upper dead band of comparator #5, (c) HP limitation in DHW production. The vertical axis has been magnified to the range 0.25–0.30.

optimal depth around $H_{BHE} = 60$ m. One interesting consequence is that relatively deep BTES will allow money savings on the surface insulation. They might be deployed even in urban areas with limited available land without jeopardizing the system performance. It seems in contradiction with early calculations that suggested an optimal borehole depth $H_{BHE} = \left(\frac{V_{BTES}}{\pi}\right)^{1/3} = \left(\frac{20000}{\pi}\right)^{1/3} \approx 18.5$ m [15]. This criteria, however, was derived from simple geometrical conditions assuming a perfectly insulated top surface. The latter point does not hold here, which may explains why the system efficiency deteriorates if the BTES gets too shallow. Besides, the insulation thickness has a negligible impact. This is in contradiction with guidelines that recommend insulating the surface [9]. The reason may be that the BTES is operated here at a much lower temperature than in classical HT-BTES (without HP), which decreases the difference of temperature between the ground and the atmosphere. The BTES is much deeper, which decreases the contact area with the atmosphere. There seems to be an optimal ground thermal conductivity λ_m around 2.0 W. K^{-1} m^{-1}, while the performance increases with the ground heat capacity $(\rho C_p)_m$. This is line with early recommendations to target ground with

medium values of λ_m and high values of $(\rho C_p)_m$ [41].

4.2.3. Thermal needs characteristics

The size of the system can be characterized by the maximum heating power $P_{heating,max}$. When it is changed, all extensive quantities (e.g. STC area, BTES and tank volumes, etc.) are scaled accordingly by a factor $P_{heating,max}/P_{heating,max,ref}$ (with $P_{heating,max,ref} = 250$ kW), while intensive quantities (e.g. spacing between boreholes) remain unchanged. $E_{ext}{}^*$ decreases when the system size increases, due to more heat being extracted from the BTES (cf. Fig. 15a). Undersizing the HP (typically below $P_{cal,HP}{}^* = 0.6$) considerably deteriorates the system performance (cf. Fig. 15b). With the control parameters udb_5 and $\Delta T_{DHW,HP}$ chosen here, the optimal nominal storage duration of DHW $\Delta t_{store,DHW}$ seems to be around 3 h (cf. Fig. 15c). Configurations with smaller tanks tends to fail reaching the DHW set point, which must be compensated by some extra external backup, while larger tanks require more heat to reach 65 °C on a daily basis.

4.2.4. Control strategy

The baseline scenario consider that solar heat can be transfer into the BTES immediately ($udb_6 = +2$ °C). The system performance can be slightly improved by increasing udb_6 to c.a. +6 °C, which postpones this heat transfer (cf. Fig. 16a). The DHW production can be slightly improved by increasing the absolute value of udb_5 to c.a. 12 °C, increasing the anticipation for DHW preparation (cf. Fig. 16b), or releasing the constraint on HP power (cf. Fig. 16b). Note that all widths of the dead bands (i.e. the difference between the upper and upper values of a comparator) are kept at 2 °C throughout the analysis.

4.3. Comparison to previous works

Panno et al. modelled a system located in Palermo (Italy) similar to the system presented in this paper, though it produces only heating and no DHW [20]. Though the thermal energy requirement is only 20% of the requirement considered here (510.5 + 226.7 = 737.2 MWh), the BTES volume was solely reduced by 38% ($V_{BTES} = 9400$ m^2 with spacing $d_{BHE} = 3$ m), while the STC area is only 8% ($S_{STC} = 200$ m^2) of the area considered in this work. The normalized electricity consumption of the pumps is then $E_{ext,w/o\ pumps}{}^* \approx 0.24$, which is very close to the value reported for our baseline scenario. The comparison enlightens that very different sizing ratios can indeed lead to similar overall efficiency. However, the results cannot be further compared, since the locations and components characteristics are not the same.

Above all, this illustrates that the comparisons between systems can only be treated through the proper exploration of the design space (with typically 10 or more parameters) and a well-defined optimization, such as the minimization of the energy cost or CO_2 content. It is not sufficient to perform one-at-a-time analysis around a reference configuration. This requires the use of some surrogate models, i.e. fast-to-run approximations of the key output of the TRNSYS models. It has been a booming topics in the energy domain for the past few years (see e.g. Ref. [42]).

5. Conclusions

The architecture and the control strategy of a system combining BTES, HP and STC for space heating and DHW preparation has been described in depth. The qualitative behaviour of the system has been verified. The main conclusions are as follows.

- For a "reference configuration" combining the three subsystems ("Design D") and characterized by $E_{heating} = 510.5$ MWh.y^{-1}, $E_{DHW} = 226.7$ MWh.y^{-1}, $V_{BTES} = 15000$ m^3, $d_{BHE} = 3$ m, $S_{STC} = 2500$ m^2, $V_{tank,sol} = 100$ m^3 and $P_{cal,HP} = 250$ kW, the system uses 274 units of gas and electricity to provide 1000 units of heating and DHW.
- This reference configuration outperforms any alternative design: Design A (STC only), Design B (STC and HP) and design C (STC and BTES) would respectively require 612, 480 and 591 units of gas and electricity to do so.
- A one-at-a-time analysis reveals that the STC area, azimuth and inclination, the solar tank volume, the BTES volume, the borehole density and the HP power are key parameters to the overall system performance. Besides, a fine tuning of the control parameters can increase the overall system performance.

A second paper will report the approximation of the key TRNSYS outputs by surrogate models, and the subsequent system optimization considering competing economic and environmental criteria.

CRediT authorship contribution statement

Charles Maragna: Conceptualization, Methodology, Validation, Formal analysis, Investigation, Writing – original draft, Writing – review & editing, Supervision. **Charlotte Rey:** Conceptualization, Methodology, Writing – review & editing, Supervision. **Marc Perreaux:** Writing – review & editing, Supervision, Project administration.

Declaration of competing interest

The authors declare the following financial interests/personal relationships which may be considered as potential competing interests: Charles MARAGNA, Charlotte REY and Marc PERREAUX report financial support was provided by the French Agency for Ecological Transition. Charles MARAGNA reports a relationship with French Ministry of Economy Finance and Recovery that includes: non-financial support. Charles MARAGNA reports a relationship with VINCI Construction SAS that includes: consulting or advisory: Charles MARAGNA took part in two research projects entirely funded by EUROVIA, a subsidiary of VINCI Construction SAS and executed by BRGM. The projects aimed at optimizing the Underground Thermal Energy Storage associated with "Power Road", a solar thermal collector embedded in roadways developed by EUROVIA. C. MARAGNA supervised one of these projects. These projects and their conclusions are not the object of the current paper.

Acknowledgments

This paper has been subsidized by the ERANET cofund GEOTHERMICA from the European Commission (grant number 731117), ADEME (French Agency for Ecological Transition, grant number 1882C0016) and RVO (the Netherlands), DETEC (Switzerland), FZJ-PtJ (Germany), EUDP (Denmark), Rannis (Iceland), VEA (Belgium), FRCT (Portugal), and MINECO (Spain). More information can be found on www.heatstore.eu. This paper would not have been possible without their support.

Annex 1: Weight coefficients to apply for the dynamic estimation of DHW

Corrections to be applied to the average DHW flow rate, following [32].

Hourly corrections				Daily corrections	
Hour of day	Mon.-Friday	Saturday	Sunday	Monday	0,96
1	1,7	1,8	1,5	Tuesday	0,94
2	0,9	1	1	Wednesday	0,98
3	0,5	0,6	0,6	Thursday	0,96
4	0,4	0,5	0,4	Friday	0,97
5	0,7	0,5	0,4	Saturday	0,98
6	1,4	0,8	0,6	Sunday	1,21
7	2,8	1,3	0,8		
8	3,9	2,6	1,3		
9	4,3	4,1	2,6		
10	5	5,9	4,5		
11	5,2	6,4	6		
12	5,7	7,1	7,1	**Monthly corrections**	
13	7	7,5	7,6	January	1,07
14	6,4	7,5	7,4	February	1,06
15	4,5	6,6	6	March	1,07
16	4	5	5,3	April	1,01
17	4,7	4,9	5	May	1,01
18	5,9	5,5	6	June	0,97
19	6,9	6,2	7,6	July	0,86
20	7,7	6,4	8,2	August	0,78
21	7,6	6,2	7,8	September	0,96
22	5,7	4,9	5,7	October	1,03
23	4,1	3,9	4	November	1,08
24	3	2,8	2,6	December	1,1

Annex 2: Derivation of HP performance map

The HP Carnot Coefficient Of Performance (COP), the maximal theoretical efficiency, is defined as:

$$\eta_{HP,Carnot} = \frac{P_{cal\ HP}}{P_{comp\ HP}} = \frac{T_{out,cond}}{T_{out,cond} - T_{out,ev}}$$

Where $P_{cal\ HP}$ is the calorific power provided by the HP, $P_{comp\ HP}$ the electrical consumption of the compressor, $T_{out,ev}$ and $T_{out,\ cond}$ the evaporator and condenser outlet temperatures respectively. A preliminary analysis of the technical data provided by CIAT manufacturer shown that their Dynaciat HP reached 50%–52% of Carnot efficiency on a broad range of evaporator and condenser temperatures. This value was retained:

$$\eta_{HP} = 0.50 \frac{T_{out,cond}}{T_{out,cond} - T_{out,ev}}$$

The HP is modelled with Type 927 with a nominal calorific power set to 250 kW for $T_{out,ev} = 0$ °C and $T_{out,\ cond} = 35$ °C. The compressor electrical consumption is kept constant throughout the whole domain at $P_{elec,ref} = 56.79$ kW. Type 927 requires $P_{cal\ HP}$ and $P_{comp\ HP}$ to be expressed as functions of $T_{in,ev}$ and $T_{in,cond}$ instead of $T_{out,ev}$ and $T_{out,\ cond}$. Therefore, for $T_{in,ev}$ and $T_{in,cond}$ in the range −20 °C to +40 °C and +20 °C to +80 °C respectively, $T_{in,ev}$ and $T_{in,cond}$ were obtained by solving the following non-linear system:

$$\begin{cases} T_{out,ev} = T_{in,ev} + \left(COP\left(T_{out,cond}, T_{out,cond}\right) - 1\right) \dfrac{P_{elec,ref}}{C_{p,fl,ev}\dot{m}_{ev}} \\ T_{out,cond} = T_{in,cond} - COP\left(T_{out,cond}, T_{out,cond}\right) \dfrac{P_{elec,ref}}{C_{p,fl,cond}\dot{m}_{cond}} \end{cases}$$

Where $C_{p,ev}$, $\dot{m}_{ev}$, $C_{p,cond}$, $\dot{m}_{cond}$ are the fluid specific heats and mass-flow rates at the evaporator and condenser. Note that a small difference of temperatures between condenser and evaporator may damage the compressor. Though no technical documentation could be found on the acceptable limit, a "recirculation zone" was modelled where the properties remain constant. A recirculation valve at the evaporator or the condenser would ensure the constraint is met. To save computational time, this was not modelled in TRNSYS, but integrated into the HP property maps.

Annex 3: Derivation of heat transfer coefficient of exchangers

All heat exchangers are counter-flow exchangers, modelled with Type 5. The heat transfer coefficients k were computed prior to TRNSYS computations with the NUT-ε method [37] to ensure a pinch $\Delta T = 2$ °C under some "nominal conditions", as follows:

$$k = \left(\dot{m}C_p\right)_{min} \times NUT \; NUT = \begin{cases} \dfrac{\varepsilon}{1-\varepsilon} & \text{if } R = 1 \\ \dfrac{1}{1-R}\log\left(\dfrac{1-\varepsilon R}{1-\varepsilon}\right) & \text{otherwise} \end{cases} \quad \left(\dot{m}C_p\right)_{min} = \min\left(\dot{m}_c C_{p,c}, \dot{m}_h C_{p,h}\right) \left(\dot{m}C_p\right)_{max} = \max\left(\dot{m}_c C_{p,c}, \dot{m}_h C_{p,h}\right) R = \frac{\left(\dot{m}C_p\right)_{min}}{\left(\dot{m}C_p\right)_{max}} \varepsilon = 1 - \frac{\Delta T}{T_{in,h} - T_{in,c}}$$

Annex 4: Mode array and output array

Mode array

			Comparators									
			1	2	3	4	5	6	7	8	9	10
	Upper input		$T_{solar,\ tank}$	$T_{heat,sp}$	$T_{solar,\ tank}$	$T_{solar,\ tank}$	$T_{DHW,sp}$	$T_{solar,\ tank}$	$T_{out,\ BTES}$	$T_{out,\ BTES}$	$T_{out,\ BTES}$	$T_{solar,\ tank}$
	Lower output		$T_{heat,sp}$	$T_{heat,\ tank}$	$T_{out,\ BTES}$	$T_{DHW,sp}$	$T_{DHW,\ tank}$	$T_{out,\ BTES}$	$T_{heat,sp}$	$T_{DHW,sp}$	$T_{out,\ BTES,\ min}$	$T_{min\ solar\ HP}$
	Upper dead band [°C]		5	−3	5	5	−10	2	7	7	2	2
	Lower dead band [°C]		3	−5	3	3	−12	0	5	5	0	0
Mode	*1*	BTES charging	−1	0	−1	−1	0	1	−1	−1	−1	−1
	2	Direct BTES discharging into heating tank (no HP)	−1	1	0	−1	−1	−1	1	−1	1	−1
	3	BTES discharging into heating tank through HP	−1	1	0	−1	−1	−1	0	−1	1	−1
	4	Direct BTES discharging into DHW tank (no HP)	−1	0	0	−1	1	−1	−1	1	1	−1
	5	BTES discharging into DHW tank through HP	−1	0	0	−1	1	−1	−1	0	1	−1
	6	Direct solar into heating tank	1	1	1	−1	−1	−1	−1	−1	−1	1
	7	Solar HP into heating tank	0	1	1	−1	−1	−1	−1	−1	−1	1
	8	Direct solar into DHW tank	−1	0	1	1	1	−1	−1	−1	−1	1
	9	Solar HP into DHW tank	−1	0	1	0	1	−1	−1	−1	−1	1

Nota: "-1" means that the comparator plays no role in the selection of this mode.

Output array

		Actuator								
Mode		transfer pump	discharging pump	charging pump	div_4, div_5	HP, div_3, HP_ev_pump, HP_cond_pump, div_10	div_7, preDHW_pump_2	div_6	BTES_pump	div_8 & preDHW_pump_1
1	BTES charging	0	0	1	0	0	0	1	1	0
2	Direct BTES discharging into heating tank (no HP)	0	1	0	0	0	0	0	1	0
3	BTES discharging into heating tank through HP	0	1	0	0	1	0	0	1	0
4	Direct BTES discharging into DHW tank (no HP)	0	1	0	0	0	1	0	1	0
5	BTES discharging into DHW tank through HP	0	1	0	0	1	1	0	1	0
6	Direct solar into heating tank	1	0	0	0	0	0	0	0	0
7	Solar HP into heating tank	1	1	0	1	1	0	1	0	0
8	Direct solar into DHW tank	1	0	0	0	0	0	0	0	1
9	Solar HP into DHW tank	1	1	0	1	1	1	1	0	0

References

[1] S. Pezzutto, M. De Felice, R. Fazeli, L. Kranzl, S. Zambotti, Status quo of the air-conditioning market in europe: assessment of the building stock, Energies 10 (2017) 1–17, https://doi.org/10.3390/en10091253.

[2] H. Lund, Renewable heating strategies and their consequences for storage and grid infrastructures comparing a smart grid to a smart energy systems approach, Energy 151 (2018) 94–102, https://doi.org/10.1016/j.energy.2018.03.010.

[3] N. Bertelsen, B.V. Mathiesen, EU-28 residential heat supply and consumption: historical development and status, Energies 13 (2020), https://doi.org/10.3390/en13081894.

[4] Ministère de la transition écologique, Quelles sont les quantités de gaz à effet de serre émises dans le monde ?, 2021. https://www.statistiques.developpement-durable.gouv.fr/edition-numerique/chiffres-cles-du-climat/partie3-quantite-de-gaz-france. (Accessed 16 July 2021).

[5] M. Lanahan, P.C. Tabares-Velasco, Seasonal thermal-energy storage: a critical review on BTES systems, modeling, and system design for higher system efficiency, Energies 10 (2017), https://doi.org/10.3390/en10060743.

[6] Drake Landing Solar Community, 2021. https://www.dlsc.ca/. (Accessed 16 July 2021).

[7] J. Nussbicker, W. Heidemann, H. Mueller-Steinhagen, Monitoring results and operational experiences for a central solar district heating system with Borehole Thermal Energy Store in Neckarsulm (Germany), in: Ecostock - 10th International Conference on Thermal Energy Storage, Richard Stockton College of New Jersey, 2006, 31.05.-02.06.2006.

[8] E. Nilsson, P. Rohdin, Performance evaluation of an industrial borehole thermal energy storage (BTES) project – experiences from the first seven years of operation, Renew. Energy 143 (2019) 1022–1034, https://doi.org/10.1016/j.renene.2019.05.020.

[9] A.J. Kallesøe, T. Vangkilde-Pedersen, HEATSTORE. Underground Thermal Energy Storage (UTES) – state-of-the-art, example cases and lessons learned, HEATSTORE Project Report, GEOTHERMICA – ERA NET Cofund Geothermal (2019) 130 (pp + appendices).

[10] F. Guo, X. Zhu, J. Zhang, X. Yang, Large-scale living laboratory of seasonal borehole thermal energy storage system for urban district heating, Appl. Energy 264 (2020), 114763, https://doi.org/10.1016/j.apenergy.2020.114763.

[11] University of Wisconsin–Madison, Solar Energy Laboratory, TRNSYS, a Transient Simulation Program, The Laboratory, Madison, Wis., 1975, 1975, https://search.library.wisc.edu/catalog/999800551102121.

[12] B. Sibbitt, D. Mcclenahan, R. Djebbar, J. Thornton, B. Wong, The Performance of a High Solar Fraction Seasonal Storage District Heating System – Five Years of Operation, vol. 00, 2012.

[13] C. Flynn, K. Sirén, Influence of location and design on the performance of a solar district heating system equipped with borehole seasonal storage, Renew. Energy 81 (2015) 377–388, https://doi.org/10.1016/j.renene.2015.03.036.

[14] F.M. Rad, A.S. Fung, M.A. Rosen, An Integrated Model for Designing a Solar Community Heating System with Borehole Thermal Storage, vol. 36, Energy for Sustainable Development, 2017, pp. 6–15, https://doi.org/10.1016/j.esd.2016.10.003.

[15] S. Lanini, F. Delaleux, X. Py, D. Nguyen, Improvement of borehole thermal energy storage design based on experimental and modelling results, Energy Build. 77 (2014) 393–400, https://doi.org/10.1016/j.enbuild.2014.03.056.

[16] F. Guo, X. Yang, Long-term performance simulation and sensitivity analysis of a large-scale seasonal borehole thermal energy storage system for industrial waste heat and solar energy, Energy Build. 236 (2021), 110768, https://doi.org/10.1016/j.enbuild.2021.110768.

[17] K.W. Tordrup, U.V. Poulsen, C. Nielsen, A modular approach to inverse modelling of a district heating facility with seasonal thermal energy storage, Energy Proc. 135 (2017) 263–271, https://doi.org/10.1016/j.egypro.2017.09.518.

[18] S. Durga, K.F. Beckers, M. Taam, F. Horowitz, L.M. Cathles, J.W. Tester, Techno-Economic Analysis of Decarbonizing Building Heating in Upstate New York Using Seasonal Borehole Thermal Energy Storage, Energy & Buildings, 2021, 110890, https://doi.org/10.1016/j.enbuild.2021.110890.

[19] A. Rosato, A. Ciervo, G. Ciampi, M. Scorpio, F. Guarino, S. Sibilio, Impact of solar field design and back-up technology on dynamic performance of a solar hybrid heating network integrated with a seasonal borehole thermal energy storage serving a small-scale residential district including plug-in electric vehicles, Renew. Energy 154 (2020) 684–703, https://doi.org/10.1016/j.renene.2020.03.053.

[20] D. Panno, A. Buscemi, M. Beccali, C. Chiaruzzi, G. Cipriani, G. Ciulla, V. Di Dio, V. Lo Brano, M. Bonomolo, A solar assisted seasonal borehole thermal energy system for a non-residential building in the Mediterranean area, Sol. Energy 192 (2019) 120–132, https://doi.org/10.1016/j.solener.2018.06.014.

[21] R. Elhashmi, K.P. Hallinan, A.D. Chiasson, Low-energy opportunity for multi-family residences: a review and simulation-based study of a solar borehole thermal energy storage system, Energy 204 (2020), 117870, https://doi.org/10.1016/j.energy.2020.117870.

[22] B. Welsch, L. Göllner-Völker, D.O. Schulte, K. Bär, I. Sass, L. Schebek, Environmental and economic assessment of borehole thermal energy storage in district heating systems, Appl. Energy 216 (2018) 73–90, https://doi.org/10.1016/j.apenergy.2018.02.011.

[23] J. Formhals, F. Feike, H. Hemmatabady, B. Welsch, I. Sass, Strategies for a transition towards a solar district heating grid with integrated seasonal geothermal energy storage, Energy 228 (2021), 120662, https://doi.org/10.1016/j.energy.2021.120662.

[24] G. Ciampi, A. Rosato, S. Sibilio, Thermo-economic sensitivity analysis by dynamic simulations of a small Italian solar district heating system with a seasonal borehole thermal energy storage, Energy 143 (2018) 757–771, https://doi.org/10.1016/j.energy.2017.11.029.

[25] N. Giordano, J. Raymond, Alternative and sustainable heat production for drinking water needs in a subarctic climate (Nunavik, Canada): borehole thermal energy storage to reduce fossil fuel dependency in off-grid communities, Appl. Energy 252 (2019), 113463, https://doi.org/10.1016/j.apenergy.2019.113463.

[26] N. Giordano, I. Kanzari, M.M. Miranda, C. Dezayes, J. Raymond, Underground Thermal Energy Storage in Subarctic Climates: a Feasibility Study Conducted in Kuujjuaq (QC, Canada), 2018, pp. 1–10, https://doi.org/10.22488/okstate.18.000024.

[27] M. Veyron, A. Voirand, N. Mion, C. Maragna, D. Mugnier, M. Clausse, Dynamic exergy and economic assessment of the implementation of seasonal underground thermal energy storage in existing solar district heating, Energy 261 (2022), 124917, https://doi.org/10.1016/j.energy.2022.124917.

[28] Y. Fan, X. Zhao, Z. Han, J. Li, A. Badiei, Y.G. Akhlaghi, Z. Liu, Scientific and technological progress and future perspectives of the solar assisted heat pump (SAHP) system, Energy 229 (2021), 120719, https://doi.org/10.1016/j.energy.2021.120719.

[29] G. Emmi, A. Zarrella, M. De Carli, A. Galgaro, An analysis of solar assisted ground source heat pumps in cold climates, Energy Convers. Manag. 106 (2015) 660–675, https://doi.org/10.1016/j.enconman.2015.10.016.

[30] Arrêté du 26 octobre 2010 relatif aux caractéristiques thermiques et aux exigences de performance énergétique des bâtiments nouveaux et des parties nouvelles de bâtiments, 2010. https://www.legifrance.gouv.fr/loda/id/JORFTEXT000022959397/. (Accessed 26 July 2021).

[31] GRETA Project, Catalogue of Operational Criteria and Constraints for Shallow Geothermal Systems in the Alpine Environment, 2017.

[32] ADEME, COSTIC, Guide technique : Les besoins d'eau chaude sanitaire en habitat individuel et collectif, 2016.

[33] T.M. Inc, MATLAB Version: 9.13.0 (R2022b), 2022. https://www.mathworks.com.

[34] D. générale de la Santé, Circulaire DGS/EA4 no 2010-448 du 21 décembre 2010 relative aux missions des agences régionales de santé dans la mise en œuvre de l'arrêté du 1er février 2010 relatif à la surveillance des légionelles dans les installations de production, de stockage et d, France, 2010.

[35] SIA, Norme suisse, in: Sondes Géothermiques. SIA 384/6, Société suisse des ingénieurs et des architectes, Zurich, 2010.

[36] BRGM, French GIS for Geothermal Energy, n.d. https://www.geothermies.fr/viewer/. (Accessed 15 September 2021).

[37] D. Marchio, P. Reboux, Introduction Aux Transferts Thermiques, 2003. Paris.

[38] Q. Xu, S. Dubljevic, Modelling and control of solar thermal system with borehole seasonal storage, Renew. Energy 100 (2017) 114–128, https://doi.org/10.1016/j.renene.2016.05.091.

[39] C. Johansson, M. Bergkvist, D. Geysen, O.D. Somer, N. Lavesson, D. Vanhoudt, Operational demand forecasting in district heating systems using ensembles of online machine learning algorithms, Energy Proc. 116 (2017) 208–216, https://doi.org/10.1016/j.egypro.2017.05.068.

[40] E. Saloux, J.A. Candanedo, Model-based predictive control to minimize primary energy use in a solar district heating system with seasonal thermal energy storage, Appl. Energy 291 (2021), https://doi.org/10.1016/j.apenergy.2021.116840.

[41] B. Sanner, High Temperature Underground Thermal Energy Storage, 1999.

[42] P. Westermann, R. Evins, Surrogate modelling for sustainable building design – a review, Energy Build. 198 (2019) 170–186, https://doi.org/10.1016/j.enbuild.2019.05.057.

[43] Norme Suisse. SIA. Sondes géothermiques. SIA 384/6, Société suisse des ingénieurs et des architectes, Zurich, 2010.